Interpreting Energy and Tracer Spectra of Upper-Ocean Turbulence in the Submesoscale Range (1–200 km)

JÖRN CALLIES

MIT/WHOI Joint Program in Oceanography, Cambridge/Woods Hole, Massachusetts

RAFFAELE FERRARI

Massachusetts Institute of Technology, Cambridge, Massachusetts

(Manuscript received 18 March 2013, in final form 13 August 2013)

ABSTRACT

Submesoscale (1–200 km) wavenumber spectra of kinetic and potential energy and tracer variance are obtained from in situ observations in the Gulf Stream region and in the eastern subtropical North Pacific. In the Gulf Stream region, steep kinetic energy spectra at scales between 200 and 20 km are consistent with predictions of interior quasigeostrophic–turbulence theory, both in the mixed layer and in the thermocline. At scales below 20 km, the spectra flatten out, consistent with a growing contribution of internal-wave energy at small scales. In the subtropical North Pacific, the energy spectra are flatter and inconsistent with predictions of interior quasigeostrophic–turbulence theory. The observed spectra and their dependence on depth are also inconsistent with predictions of surface quasigeostrophic–turbulence theory for the observed ocean stratification. It appears that unbalanced motions, most likely internal tides at large scales and the internal-wave continuum at small scales, dominate the energy spectrum throughout the submesoscale range. Spectra of temperature variance along density surfaces, which are not affected by internal tides, are also inconsistent with predictions of geostrophic-turbulence theories. Reasons for this inconsistency could be the injection of energy in the submesoscale range by small-scale baroclinic instabilities or modifications of the spectra by coupling between surface and interior dynamics or by ageostrophic frontal effects.

1. Introduction

Oceanographers have long debated how energy is transferred from large to dissipative scales. Much progress has been made in describing the energy pathways from basin to mesoscales and then from scales on the order of 1 km down to millimeter scales.[1] But our understanding of the transfer in between, in the submesoscale range, is still rudimentary.[2] A major question is whether the energy fluxes in the submesoscale are dominated by internal waves and other unbalanced motions or whether there is an important contribution by geostrophic motions. The geostrophic part of submesoscale motions has received much attention in theoretical studies over the past decade (e.g., Lapeyre and Klein 2006), but supporting analysis of observations is lacking. Our goal here is to use available observations from the upper-midlatitude ocean to test different theories of submesoscale dynamics.

Oceanic motions can easily be separated in the frequency domain. Figure 1 shows an example frequency spectrum from a mooring in the subtropical North Pacific [the data are available at http://cmdac.oce.orst.edu/; Schmitz (1988)]. Geostrophically balanced flows span the range of frequencies below the inertial frequency f, inertial oscillations are visible as a broad peak around f, the M_2 lunar tide appears as a sharp superinertial peak, and a broad-band internal-wave continuum spans the frequency range between f and the buoyancy frequency N. It is much less clear how these motions project onto spatial scales. This is a serious limitation to our understanding of submesoscale turbulence

[1] All scales are given as wavelengths.

[2] We use the term "submesoscale" to designate the range 1–200 km, roughly the scales below the first deformation radius. There are other uses of the term in the literature, which are based on order-1 Rossby and Richardson numbers. We here attempt to understand what the dynamics of these scales are, so we use submesoscale to designate the range of scales without presupposing their dynamics.

Corresponding author address: Jörn Callies, Massachusetts Institute of Technology, 77 Massachusetts Ave., Cambridge, MA 02139.
E-mail: joernc@mit.edu

DOI: 10.1175/JPO-D-13-063.1

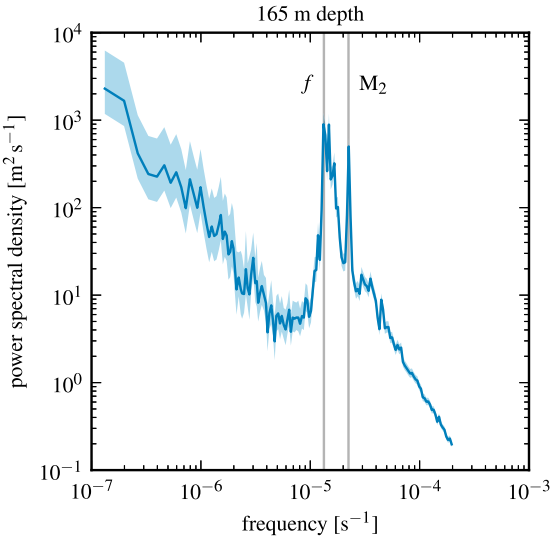

FIG. 1. Frequency spectrum of kinetic energy from mooring WHOI 794 at 35°N, 152°W (October 1983–September 1985). Marked are f and M_2. Shading shows 95% confidence intervals.

because the interaction of modes across spatial scales is at the core of turbulence theories.

It is generally believed that the kinetic energy in the midlatitude upper ocean is dominated by geostrophic eddies at scales larger than the first baroclinic deformation scale—the wavelength associated with the deformation radius—of about 50–200 km and by internal waves at scales below 1 km. We here attempt to understand the range of scales in between, the submesoscale range, using wavenumber spectra of kinetic energy, potential energy, and tracer variance, together with their vertical variations. Is most of the submesoscale variability balanced or unbalanced? Do our theories of geostrophic turbulence successfully describe the balanced part of the flow? Previous attempts to test these theories remain largely inconclusive (e.g., Samelson and Paulson 1988; Stammer 1997; Le Traon et al. 2008).

To answer these questions, we analyze two in situ datasets in two different dynamical regimes: the Oleander dataset (Wang et al. 2010) in the Gulf Stream region and the Spice dataset (Ferrari and Rudnick 2000) in the eastern subtropical North Pacific (Fig. 2). The Gulf Stream is a strong baroclinic current with an associated deep reversal of the potential vorticity (PV) gradient. This induces deep Phillips-type baroclinic instability and strong mesoscale eddy activity (e.g., Tulloch et al. 2011). In the North Pacific, in the quiescent subtropical gyre, on the other hand, interior-PV gradients are weak. A surface-buoyancy gradient persists, however, so one might expect shallow instabilities and surface-frontal dynamics to play a prominent role there. Lapeyre and Klein (2006) suggested that surface-quasigeostrophic (QG) turbulence (Blumen 1978) may be the relevant framework for interpreting the submesoscale turbulence that develops in response to frontogenesis.

In the Gulf Stream region, we find spectra consistent with interior-QG turbulence (Charney 1971) at scales larger than 20 km and consistent with internal-wave dynamics at smaller scales. In the subtropical North Pacific, the observations are inconsistent with existing geostrophic-turbulence theories. There is indication that internal tides play an important role at scales as large as

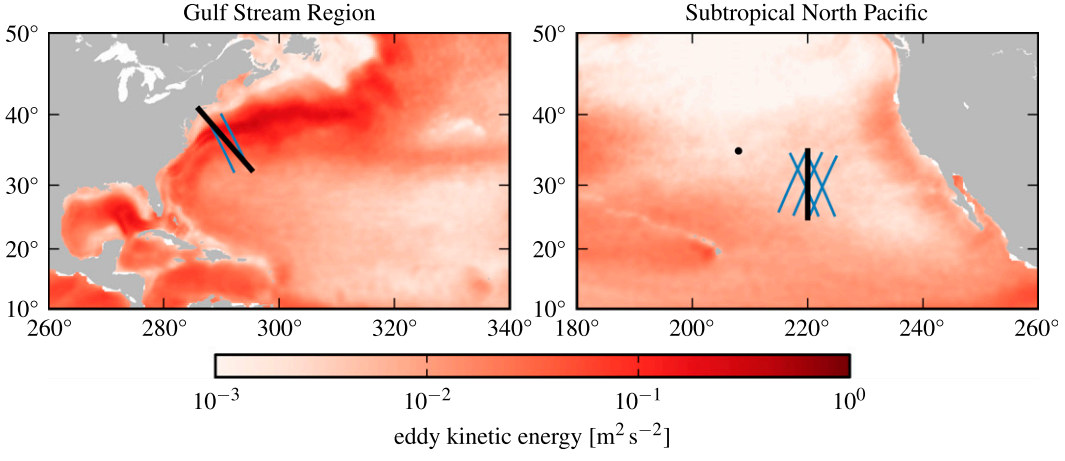

FIG. 2. Tracks along which measurements were collected in the (left) Oleander and (right) Spice experiments (thick black lines). The satellite tracks used in the analysis are shown as thin blue lines. The site of the mooring used for Fig. 1 is marked with a black dot. The background color is a map of eddy kinetic energy from the Archiving, Validation, and Interpretation of Satellite Oceanographic data (AVISO) gridded altimetry.

100 km. At small scales, the internal-wave continuum again dominates.

The paper is organized as follows. In section 2, we review the existing theoretical predictions for the spectra of balanced and unbalanced flows. In section 3, we discuss how these predictions relate to spectra computed from one-dimensional transects. We review previous observations in section 4. In sections 5 and 6, we introduce and compare against the theoretical predictions the two sets of observations. We discuss implications in section 7. The appendix examines surface QG–turbulence predictions for wavenumber spectra and their vertical dependence in nonconstant stratification.

2. Theoretical predictions for submesoscale wavenumber spectra

We here review theories that have been proposed to describe submesoscale turbulence. Two variants of geostrophic-turbulence theory have been put forward: interior-QG turbulence (Charney 1971), resulting from deep baroclinic instabilities, and surface-QG turbulence (Blumen 1978), developing in response to frontogenesis. That discussion (e.g., Stammer 1997; Le Traon et al. 2008; Wang et al. 2010), however, has largely ignored the internal-wave field emphasized in earlier works (e.g., Katz 1973). The internal-wave continuum, as well as tides, inertial oscillations, and mixed layer flows, may contribute significantly to submesoscale variability. A substantial theory only exists for the internal-wave continuum. The other unbalanced flows nevertheless have certain characteristics that can be used to assess their relative importance.

a. Geostrophic turbulence

The theories for submesoscale-geostrophic turbulence assume that energy is extracted from the mean flow through baroclinic instability at scales close to the deformation scale, which in the midlatitude ocean generally lies at the large-scale end of what we call the submesoscale range. It is further assumed that dissipation is negligible throughout the submesoscale range, so that nonlinear interactions between modes transfer energy and enstrophy across a submesoscale inertial range. If the turbulence is horizontally homogeneous and isotropic, Kolmogorov-like dimensional arguments can be used to deduce spectral slopes of horizontal kinetic energy $\mathcal{K} = \langle u^2 + v^2 \rangle/2$ and potential energy $\mathcal{P} = (\langle b^2 \rangle/N^2)/2$ in wavenumber space, where u and v are a pair of orthogonal horizontal velocity components, b is buoyancy, N is the background stratification, and $\langle \cdot \rangle$ is the two-dimensional spatial average. The two-dimensional isotropic spectra will be denoted by $\mathcal{K}_{k_h}$ and $\mathcal{P}_{k_h}$, where $k_h = (k^2 + l^2)^{1/2}$ is the magnitude of the horizontal wavenumber. From the spectral slope of kinetic energy, the spectral slope of the variance of a passive tracer $\mathcal{T} = \langle c^2 \rangle/2$ can also be inferred, where c denotes the tracer concentration. Because the motion is quasigeostrophic and therefore along isopycnals, all of these spectra are to be understood as along isopycnals.

Any QG flow can be decomposed into a component due to interior-PV anomalies and a component due to surface-buoyancy anomalies (e.g., Lapeyre and Klein 2006). Charney (1971) considered QG flows resulting from interior-PV anomalies that are far enough from boundaries that the effect of the surface-buoyancy anomalies can be ignored. In the submesoscale inertial range, potential enstrophy is then cascaded down to small scales. It follows that the spectra of kinetic and potential energy scale like $\mathcal{K}_{k_h} \sim \mathcal{P}_{k_h} \sim k_h^{-3}$.[3]

Interior QG–turbulence scalings, as already noted by Charney, do not apply at and near the ocean surface. As a complement, Blumen (1978) considered a flow that has a uniform interior PV and is thus entirely associated with surface-buoyancy anomalies. This limit is commonly referred to as surface QG. In an ocean with constant stratification, the surface spectra of kinetic and potential energy in the submesoscale inertial range are relatively flat: $\mathcal{K}_{k_h} \sim \mathcal{P}_{k_h} \sim k_h^{-5/3}$.

In constant stratification, surface-QG motions of horizontal scale $2\pi/k_h$ have a vertical decay scale f/Nk_h. Modes with horizontal scales smaller than $-Nz/f$ have decayed significantly at a given depth z, while larger-scale modes are essentially unattenuated. Surface-QG turbulence thus predicts kinetic and potential energy spectra to follow the surface spectra above this transition scale and

[3] Charney gave the three-dimensional isotropic spectra $\mathcal{K}_K$ and $\mathcal{P}_K$, where $K = (k^2 + l^2 + f^2 m^2/N^2)^{1/2}$ is the magnitude of the three-dimensional wavenumber with the vertical wavenumber m rescaled by f/N. A three-dimensional isotropic spectrum $\mathcal{S}_K$ is related to the two-dimensional isotropic spectrum $\mathcal{S}_{k_h}$ by (cf. Batchelor 1953)

$$\mathcal{S}_{k_h} = k_h \int_{k_h}^{\infty} \frac{\mathcal{S}_K}{K(K^2 - k_h^2)^{1/2}}\, dK.$$

If the three-dimensional spectrum locally follows the power law $\mathcal{S}_K = AK^{-n}, n > -1$, and has a slope <1 at higher wavenumbers, then the integral above is dominated by low wavenumbers:

$$\mathcal{S}_{k_h} \approx Ak_h \int_{k_h}^{\infty} \frac{K^{-n}}{K(K^2 - k_h^2)^{1/2}}\, dK = A' k_h^{-n} \quad \text{with}$$

$$A' = A \int_1^{\infty} \frac{\kappa^{-(n+1)}}{(\kappa^2 - 1)^{1/2}}\, d\kappa.$$

In this case, the two-dimensional spectrum follows the same power law as the three-dimensional one. The spectral slopes given by Charney therefore directly translate to the two-dimensional spectra.

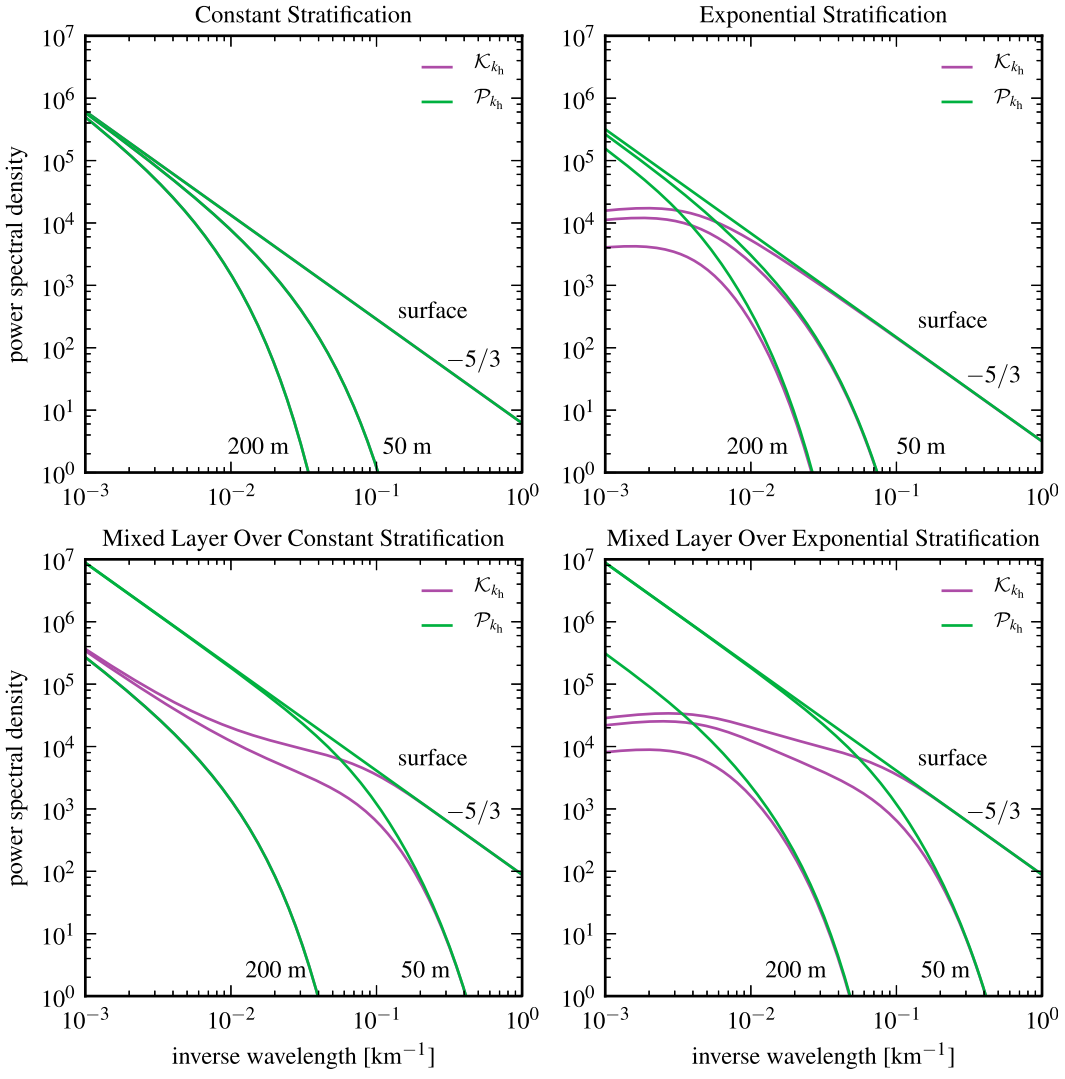

FIG. 3. Surface QG–turbulence predictions of two-dimensional isotropic wavenumber spectra of kinetic and potential energies at the surface and at depths 50 and 200 m for (top left) constant stratification, (top right) exponential stratification, (bottom left) a mixed layer of 100-m depth overlying constant stratification, and (bottom right) a mixed layer of 100-m depth overlying exponential stratification.

rapidly decay below [see our Fig. 3, described in greater detail below, and Scott (2006)]. At any given depth, we might expect surface-QG turbulence to prevail at large scales, but interior-PV anomalies to become important at small scales—with the transition scale depending on depth. This prediction was found to be consistent with idealized primitive equation model simulations (Klein et al. 2008).

In an ocean with nonconstant stratification, the surface QG–turbulence predictions for energy spectra significantly differ from the case of constant stratification. In exponential stratification, the kinetic energy spectra are flatter at scales larger than the deformation scale Nd/f associated with the depth scale d of stratification (see Fig. 3 and the appendix). An overlying mixed layer further changes the predictions, leading to a flattening of the kinetic energy spectra at scales larger than the deformation scale $N_{\mathrm{ML}}h/f$ associated with the depth of the mixed layer h and to drastically decreased energy levels in the thermocline compared to the mixed layer (see Fig. 3 and the appendix).

In turbulent inertial ranges as described above, there is a relationship between the kinetic energy spectrum and the variance spectrum of a conservative passive tracer stirred by the turbulence (e.g., Vallis 2006). If the kinetic energy spectrum rolls off as $\mathcal{K}_{k_h} \sim k_h^{-n}$ for $n < 3$, the associated passive-tracer spectrum rolls off as $\mathcal{T}_{k_h} \sim k_h^{(n-5)/2}$. For kinetic energy spectra steeper than

-3, the tracer stirring is nonlocal and a Batchelor spectrum $\mathcal{T}_{k_h} \sim k_h^{-1}$ emerges. In interior-QG turbulence, where the kinetic energy spectrum rolls off as $\mathcal{K}_{k_h} \sim k_h^{-3}$, the passive tracer thus undergoes strong filamentation and develops a spectrum $\mathcal{T}_{k_h} \sim k_h^{-1}$. In surface-QG turbulence, on the other hand, where the surface–kinetic energy spectrum is $\mathcal{K}_{k_h} \sim k_h^{-5/3}$ or flatter, the more energetic smaller-scale eddies mix the tracer more effectively at smaller scales and the variance spectrum is correspondingly steeper: $\mathcal{T}_{k_h} \sim k_h^{-5/3}$ or steeper. At depth, however, the variance spectrum develops a Batchelor spectrum $\mathcal{T}(k_h) \sim k_h^{-1}$ at the smaller submesoscales, where the surface modes have decayed at the given depth (Scott 2006).

The surface-QG framework is useful to study geostrophic turbulence in the upper ocean. The scaling laws predicted by surface QG–turbulence theory, however, need to be revised to account for important ageostrophic corrections (Capet et al. 2008b). The flat kinetic and potential energy spectra in surface-QG turbulence are indicative of the creation of strong horizontal shears and sharp buoyancy gradients, the prelude to frontogenesis (Hoskins and Bretherton 1972). If one includes advection by the ageostrophic part of the velocity in Blumen's idealized flow (a term ignored in surface-QG theory), discontinuities form in both the velocity and buoyancy fields, and the energy spectra become $\mathcal{K}_{k_h} \sim \mathcal{P}_{k_h} \sim k_h^{-2}$ (Boyd 1992). If a passive tracer is stirred by a discontinuous flow field, it also develops discontinuities and its variance spectrum consequently scales like $\mathcal{T}_{k_h} \sim k_h^{-2}$.

Beyond the changes in spectral slopes, frontogenesis and ageostrophic motion can significantly change the energy cascade. Molemaker et al. (2010) show that ageostrophic flows are responsible for reversing the direction of the energy cascade of a surface QG–like flow from upscale in the QG limit to downscale in a Boussinesq system that allows frontogenesis.

b. The internal-wave continuum

Starting with the seminal work of Garrett and Munk (1972), it was realized that internal waves are characterized by a continuum spectrum spanning frequencies from f to N, over which a few spectral peaks due to tides and inertial motions are superimposed. The internal-wave continuum spectrum is understood to be set through weak interactions of linear waves (e.g., Lvov et al. 2004). It is remarkably uniform across the ocean and has been shown to be successfully described by the empirical model spectra of Garrett and Munk (GM; e.g., Munk 1981). The GM spectra predict the spectral densities of the kinetic and potential energies as functions of frequency and vertical wavenumber; they can be converted to horizontal wavenumber space using the dispersion relation of internal waves and summing over all vertical wavenumbers (e.g., Klymak and Moum 2007). These wavenumber spectra scale like $\mathcal{K}_{k_h} \sim \mathcal{P}_{k_h} \sim k_h^{-2}$ in the short-wave limit and flatten out at scales larger than about 10 km (as shown, for example, by the dotted purple line in Fig. 5, described in greater detail below).

The GM spectra can also be used to deduce the passive-tracer variance generated by the internal-wave continuum, on both horizontal and isopycnal surfaces. For tracers with vertical gradients much larger than isopycnal gradients, like temperature or salinity, the tracer variance on horizontal surfaces is dominated by distortions of the vertical background gradient. We can then estimate $\hat{c} = (\partial C/\partial z)\hat{\zeta} = (\partial C/\partial z)\hat{b}/N^2$, so that $\mathcal{T} = (\partial C/\partial z)^2\mathcal{P}/2N^2$, where C is the background tracer field, and $\zeta = b/N^2$ is the vertical displacement due to the wave. Along isopycnals, this variance is filtered out and we are left with displacements of the much weaker isopycnal gradient. The associated variance can be estimated analogously by considering the isopycnal wave-induced displacements and is typically several orders of magnitude smaller. Both vertical and along-isopycnal displacements generate a tracer spectrum that scales like $\mathcal{T}_{k_h} \sim k_h^{-2}$ in the short-wave limit and flattens out at scales larger than about 10 km.

c. Tides

Barotropic tides are generated by astronomical forces; baroclinic (internal) tides are forced by barotropic tides flowing over topography. These baroclinic tides are not included in the GM spectra and the associated kinetic energy varies considerably between geographical locations (e.g., Arbic et al. 2012).

Both barotropic and baroclinic tides have a specific frequency that is set by the forcing, so that linear theory can be used to deduce the horizontal wavenumbers baroclinic tides project onto (e.g., Dushaw et al. 1995). Altimetric observations and high-resolution simulations show that baroclinic tides appear as somewhat broadened peaks in wavenumber spectra, to the extent that they may be better described as broad-band signals (e.g., Ray and Mitchum 1997; Zhao et al. 2012; Richman et al. 2012). A theory that explains this signature in wavenumber spectra is lacking and in situ observations are difficult because of the tides' large spatial scales and high frequencies.

d. Inertial oscillations

The ocean is nearly resonant at the inertial frequency. Variable winds therefore easily excite inertial oscillations in the upper ocean, particularly in the mixed layer (e.g., Pollard 1970). The oscillations are quasi-two-dimensional and have the frequency of the Coriolis parameter f. The internal-wave dispersion relation for waves of frequency f

TABLE 1. Properties of one-dimensional wavenumber spectra ($\mathcal{K}_k^T$ and $\mathcal{K}_k^L$ are the transverse and longitudinal kinetic energy spectra, $\mathcal{P}_k$ is the potential energy spectrum, and $\mathcal{T}_k$ is the variance spectrum of a passive tracer).

	QG turbulence			
	Interior	Surface (constant N)	Surface (nonconstant N)	Internal-wave continuum
$\mathcal{K}_k^T$ slope	-3	$-5/3$ (at surface, steep below; see Fig. 3)	(see Fig. 4)	-2 (in small-scale roll off)
Relation between $\mathcal{K}_k^T$ and $\mathcal{K}_k^L$	$\mathcal{K}_k^T = 3\mathcal{K}_k^L$	$\mathcal{K}_k^T = 5/3\mathcal{K}_k^L$ (at surface)	(see Fig. 4)	$\mathcal{K}_k^T = \mathcal{K}_k^L$
Relation between $\mathcal{P}_k$ and $\mathcal{K}_k^T$ and $\mathcal{K}_k^L$	$\mathcal{P}_k = \mathcal{K}_k^L$	$\mathcal{P}_k = \mathcal{K}_k^L + \mathcal{K}_k^T$	(see Fig. 4)	(see Fig. 6)
$\mathcal{T}_k$ slope	-1	$-5/3$ (at surface; flatter below)	(steep at surface, flat below)	-2 (in short-wave roll off, weak stirring along isopycnals)

predicts that the waves have an infinite horizontal scale. Some spreading in frequency results from changes in f with latitude and from the background vorticity. As a result, the inertial oscillations are characterized by a broad peak in the frequency spectrum (e.g., Garrett 2001) and have large horizontal scales, but a theory predicting their signature in wavenumber spectra does not exist. The quasi-two-dimensional nature of inertial oscillations, however, implies a large kinetic–to-potential energy ratio. This is not what we find in the observations, as discussed in section 6.

e. Mixed layer flows

In addition to superinertial waves, the wind forces subinertial variability in the upper ocean. If the wind field is spatially variable, it transfers its variability to the Ekman currents. The resultant wavenumber spectrum depends on the wavenumber spectrum of the winds, which is reddened in the transfer (Frankignoul and Müller 1979). Additional spatial variability is generated by the vorticity of balanced flows (e.g., Niiler 1969).

Other sources of surface-intensified turbulence are mixed layer instabilities. Both symmetric instability (e.g., Emanuel 1994) and mixed layer baroclinic instability (e.g., Blumen 1979) generate turbulent flows in the mixed layer (Haine and Marshall 1998). The most baroclinically unstable mode has a horizontal scale on the order of 1–10 km (Boccaletti et al. 2007). Theory (Fox-Kemper et al. 2008), modeling (e.g., Capet et al. 2008b), and observations (Shcherbina et al. 2013) indicate that these mixed layer instabilities can substantially enhance submesoscale energy in the presence of a deep winter mixed layer. Such mixed layer flows have energy spectra close to k_h^{-2}. The dynamics are distinct from surface QG and are better described as Eady-like, with eddies confined between the surface and the strong PV gradient at the mixed layer base.

The mixed layer also features small-scale wind- and buoyancy-driven turbulence (e.g., Kantha and Clayson 2000). These flows typically have aspect ratios close to one and scales that are generally smaller than what we defined as the submesoscale range.

All these flows are strong in the mixed layer and decay rapidly below. As discussed in sections 5 and 6, this is not what we find in the observations presented here: the energy levels in mixed layer and thermocline are very similar.

3. Relating two-dimensional spectral theories to one-dimensional spectral observations

All predictions reviewed above are for two-dimensional isotropic spectra. Observations, however, are more typically taken along a one-dimensional track. In such cases, only one-dimensional spectra can be computed as functions of the longitudinal (along track) wavenumber, say k.[4] The conversion of a two-dimensional isotropic spectrum $\mathcal{S}_{k_h}$ to a one-dimensional spectrum $\mathcal{S}_k$ is given by (cf., Batchelor 1953)

$$\mathcal{S}_k = \frac{2}{\pi}\int_k^\infty \frac{\mathcal{T}_{k_h}}{(k_h^2 - k^2)^{1/2}}\, dk_h. \tag{1}$$

If the two-dimensional spectrum locally follows a power law $\mathcal{S}_{k_h} \sim k_h^{-n}$, $n > 0$, and remains red at higher wavenumbers, then the one-dimensional spectrum follows the same power law $\mathcal{S}_k \sim k^{-n}$.[5] The predicted scalings given above thus directly translate to the one-dimensional spectra of kinetic energy, potential energy, and tracer variance, summarized in Table 1.

It is important to realize, however, that for an isotropic flow, the one-dimensional spectra of the longitudinal

[4] We use "longitudinal" exclusively in this sense and never in the sense of "zonal."

[5] The integral in (1) is then dominated by low wavenumbers, where $\mathcal{S}_{k_h} = Ak_h^{-n}$, and can be approximated by

$$\mathcal{S}_k \approx \frac{2}{\pi}\int_k^\infty \frac{Ak_h^{-n}}{(k_h^2 - k^2)^{1/2}}\, dk_h = A'k^{-n} \quad \text{with}$$

$$A' = \frac{2}{\pi}A\int_1^\infty \frac{\kappa^{-n}}{(\kappa^2 - 1)^{1/2}}\, d\kappa.$$

(along track) and transverse (across track) components of kinetic energy, $\mathcal{K}^L = \langle u^2 \rangle/2$ and $\mathcal{K}^T = \langle v^2 \rangle/2$, are not necessarily equal (u and v are the longitudinal and transverse horizontal velocity components, respectively). Instead, for an isotropic two-dimensional (meaning horizontally nondivergent) flow, they satisfy

$$\mathcal{K}^T_k = -k \frac{d}{dk} \mathcal{K}^L_k , \tag{2}$$

so that for a spectrum $\mathcal{K}_{k_h} \sim k_h^{-n}$, the relation between transverse and longitudinal spectra is $\mathcal{K}^T_k = n\mathcal{K}^L_k$ (e.g., Batchelor 1953; Leith 1971; Charney 1971).[6]

Relation (2) is particularly relevant for geostrophic turbulence because those flows are horizontally nondivergent at leading order. In addition, QG buoyancy is related to the vertical gradient of the streamfunction and therefore the one-dimensional potential energy spectrum is also related to the components of the one-dimensional kinetic energy spectrum. In interior-QG turbulence, the potential energy spectrum equals the longitudinal component of the kinetic energy spectrum $\mathcal{P}_k = \mathcal{K}^L_k$ (Charney 1971), whereas in surface-QG turbulence it equals the total kinetic energy spectrum $\mathcal{P}_k = \mathcal{K}^L_k + \mathcal{K}^T_k$ in the case of constant stratification. For more realistic stratification, surface-QG turbulence predicts the kinetic energy levels to be lower than the potential energy levels at scales larger than the deformation scale (Fig. 4, see the appendix).

In an internal-wave field, the flow is three-dimensional—so (2) does not hold in general.[7] If the wave field is horizontally isotropic, as assumed in Garrett and Munk (1972), we instead expect the one-dimensional longitudinal and transverse kinetic energy spectra to be equal (i. e., $\mathcal{K}^L_k = \mathcal{K}^T_k$). The same is true for an isotropic internal-tide field.

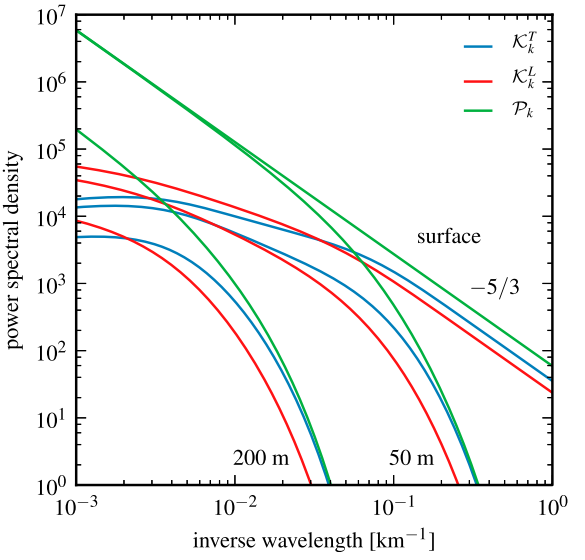

FIG. 4. Surface QG–turbulence predictions of one-dimensional wavenumber spectra of longitudinal and transverse kinetic energy and potential energy at the surface and at 50- and 200-m depths for a mixed layer of 100-m depth overlying exponential stratification.

Ageostrophic circulations at fronts, Ekman flows, and mixed layer turbulence are all characterized by strong vertical velocities and are far from two-dimensional. Hence, (2) is not expected to hold for these flows. Because of anisotropies, however, $\mathcal{K}^T_k \neq \mathcal{K}^L_k$ is likely.

The main point here is that considering the longitudinal and transverse components of the kinetic energy spectrum separately yields additional ways to discriminate between the different regimes of geostrophic turbulence and between two- and three-dimensional motions. These relationships are particularly useful because the spectral slopes are often quite similar for the different regimes.

4. Review of previous observations of submesoscale spectra

a. *In situ observations*

Early observations of wavenumber spectra of potential energy in the submesoscale range were often interpreted in terms of internal-wave variability. Katz (1973) reported on tow experiments in the Sargasso Sea thermocline and showed that spectra on scales between about 50 km and 30 m scaled close to $\mathcal{P}_k \sim k^{-2}$. He discussed their relation to the GM model spectra, which were later modified to be consistent with these observations (Garrett and Munk 1975).

[6] They are related to the two-dimensional isotropic spectrum $\mathcal{K}_{k_h}$ by

$$\mathcal{K}^L_k = \frac{2}{\pi} \int_k^\infty \frac{(k_h^2 - k^2)^{1/2} \mathcal{K}_{k_h}}{k_h^2} dk_h \quad \text{and}$$

$$\mathcal{K}^T_k = \frac{2}{\pi} k^2 \int_k^\infty \frac{\mathcal{K}_{k_h}}{k_h^2 (k_h^2 - k^2)^{1/2}} dk_h .$$

[7] For motions of frequency $f < \omega < N$, it follows from the Wentzel–Kramers–Brillouin (WKB) solution of the linear Boussinesq equations that there is significant vertical divergence: the ratio of the sum of the magnitudes of the terms of the horizontal divergence, $\partial u/\partial x$ and $\partial v/\partial y$, to the magnitude of the vertical divergence, $\partial w/\partial z$, satisfies

$$\frac{1}{2} \frac{\omega^2 + f^2}{\omega^2} \leq \frac{k^2 |\hat{u}|^2 + l^2 |\hat{v}|^2}{m^2 |\hat{w}|^2} \leq 1 .$$

It must therefore be of order unity, which implies that $|\partial w/\partial z|$ is of the same order as $|\partial u/\partial x|$ and $|\partial v/\partial y|$.

After the Mid-Ocean Dynamics Experiment and the discovery of the mesoscale, submesoscale wavenumber spectra have increasingly been interpreted as manifestations of geostrophic turbulence. Samelson and Paulson (1988) presented wavenumber spectra from the subtropical North Pacific and found that potential energy spectra scaled close to $\mathcal{P}_k \sim k^{-2}$ at scales 10–100 km and close to $\mathcal{P}_k \sim k^{-3}$ at scales 1–10 km in the mixed layer (15-m depth); in the thermocline (70-m depth), they found $\mathcal{P}_k \sim k^{-2}$ at scales 1–100 km. They concluded that the spectral slopes are consistent with interior-QG turbulence dominating in the mixed layer and internal-wave variability dominating in the thermocline. The steep spectrum in the mixed layer, however, was not confirmed by an experiment conducted a few degrees further east and on an even wider range of scales (Ferrari and Rudnick 2000). The potential energy spectra were instead reported to scale close to $\mathcal{P}_k \sim k^{-2}$ in both the mixed layer and thermocline.

Wang et al. (2010) analyzed a long-term dataset of mixed layer velocities and temperatures in the Gulf Stream region, along a transect between New York Harbor and Bermuda. They found that the energy spectra fall off approximately like $\mathcal{K}_k \sim \mathcal{P}_k \sim k^{-3}$ on scales between 250 and 20 km, consistent with interior-QG turbulence. They also reported that the power spectra of the zonal and meridional velocities are similar and interpreted this result as evidence of horizontal isotropy. The similarity between the power spectra of kinetic and potential energies was further interpreted as a signature of energy equipartition. As pointed out in the theoretical review, however, a more stringent test of whether the flow is two-dimensional and isotropic relies on the comparison of spectra of the longitudinal and transverse components of kinetic energy—a test we will explore in this paper. Furthermore, interior-QG turbulence predicts an equipartition between the longitudinal component of kinetic energy and potential energy ($\mathcal{K}_k^L = \mathcal{P}_k$), not between the total kinetic energy (i.e., $\mathcal{K}_k$) and potential energy (i.e., $\mathcal{P}_k$).

Wang et al. (2010) ignored scales below 20 km and measurements below the base of the mixed layer, where internal waves are expected to become dominant. A major goal of this paper will be to provide a comprehensive analysis of spectra in the mixed layer and below on scales from a few hundred kilometers down to 1 km (resolution permitting). Comparing different depths and scales allows a more robust assessment of what dynamics dominate the submesoscale range in different places.

b. Altimetry observations

The advent of satellite altimetry sparked numerous investigations of surface–kinetic energy spectra. The Ocean Topography Experiment (TOPEX)/Poseidon[8] and *Jason-1/2* altimeters measured the sea surface height (SSH) along tracks spanning the global oceans from 65°N to 65°S. After correcting for instrument and atmospheric noise and removing the contribution of barotropic tides, geostrophic balance is routinely applied to convert the SSH measurements to transverse geostrophic velocities at the sea surface, from which the transverse component of the geostrophic surface–kinetic energy spectrum can be estimated. Stammer (1997) found this spectrum to fall off like $\mathcal{K}_k^T \sim k^{-3}$ throughout the extratropical oceans, consistent with interior-QG turbulence. Le Traon et al. (2008) instead found the spectra in major current regions to be closer to $\mathcal{K}_k^T \sim k^{-5/3}$ and concluded that surface-QG turbulence is the more relevant dynamical framework.

Xu and Fu (2011, 2012) used *Jason-1/2* along-track data to create a global map of spectral slopes of surface-kinetic energy on scales between 250 and 70 km. They found large geographical differences with relatively steep spectra in the major current regions (between k^{-2} and $k^{-2.5}$) and flatter spectra in the rest of the extratropical oceans (between k^0 and $k^{-1.5}$). These slopes are everywhere smaller than those inferred from in situ observations. One possible explanation is that the estimates of Xu and Fu, despite the attempt to remove instrumental noise, are still contaminated by noise at scales that are only marginally resolved by altimeters. This was corroborated by the modeling results of Sasaki and Klein (2012) and Richman et al. (2012), who found steeper spectra than the altimetric ones in regions of low mesoscale activity. A second possibility is that ageostrophic flows, like internal tides, have an important signature in SSH, so that velocities inferred from SSH using geostrophic balance are not accurate (Richman et al. 2012). A third possibility is that in situ observations are dominated by ageostrophic flows not measured by altimeters.

In summary, the surface–kinetic energy spectra inferred from altimetry, which only account for the geostrophic part of the flow (possibly contaminated by ageostrophic flow that projects onto SSH), are steeper in major current regions than in quiescent gyres. Spectra inferred from in situ measurements, which account for the full geostrophic plus ageostrophic flow, confirm this tendency, but the actual slopes differ substantially. Here we try to unravel what dynamics

[8] "Poseidon" can stand for "Premier Observatoire Spatial Étude Intensive Dynamique Océan et Novosphère (sic)" or "Positioning Ocean Solid Earth Ice Dynamics Orbiting Navigator" (Wunsch and Stammer 1998).

dominate the submesoscale in different geographical regions and at different depths, analyzing in situ data with a broad set of diagnostics: (i) the longitudinal and transverse components of kinetic energy spectra, (ii) the potential energy spectra, (iii) the variance spectra of passive tracers, and (iv) the changes of the spectra with depth.

5. Gulf Stream region

a. Oleander dataset

We revisit the Oleander dataset, previously analyzed by Wang et al. (2010), to provide a more thorough test of whether the dynamics are consistent with geostrophic-turbulence theories (the data are available at http://po.msrc.sunysb.edu/Oleander/). Furthermore, we investigate whether a transition to an internal-wave regime occurs at scales below 20 km that were not analyzed in Wang et al. (2010).

The ADCP data were collected on repeat transects from New York Harbor to Bermuda (Fig. 2) between 1994 and 2009. We use data at 39-m depth, which is within the mixed layer, and at 150-m depth, which is below the base of the mixed layer except during a few occasions of strong convection in winter. We do not choose a deeper level to retain good statistics; data gaps become more frequent at greater depths. We make the common fast-tow approximation that assumes the fields to be frozen in time over the course of a transect. It takes 20 min to cover 10 km and 3.5 h to cover 100 km at a ship speed of about $8\,\mathrm{m\,s^{-1}}$. Geostrophic eddies have generally longer time scales (e.g., Stammer 1997) and are well resolved. Internal waves have periods larger than $2\pi/N = 20$ min and this high-frequency component projects onto small horizontal scales. Waves with larger horizontal scales have larger periods so that the frozen-field approximation is also well justified for the internal-wave continuum (cf. Garrett and Munk 1972). The approximation becomes problematic for tidal flows with large horizontal scales, for which aliasing will occur.

We select transects at least 1000-km long and with data gaps no wider than 10 km (311 transects in the mixed layer and 264 in the thermocline), and use cubic splines to interpolate onto a 2.5 km regular grid, which is about the spacing of the original data. Even though the presence of the Gulf Stream renders the velocity field statistically inhomogeneous, we use the full transects; discarding the part of the transects that includes the Gulf Stream does not give qualitatively different results. We also disregard seasonal variations—the qualitative characteristics of the spectra are independent of season in this dataset. More recent data from the same transect, but collected with a different instrument, do show a seasonal cycle with more energetic small scales in the winter mixed layer. The results in this paper should therefore be regarded as representative of times with no deep mixed layer. We rotate the velocities into the reference frame of the ship track to separate the longitudinal and transverse components. We divide the transects into three segments with a 50% overlap, apply a Hann window, and calculate the discrete Fourier transform of each segment. We average the resulting Fourier transforms over the three segments and 10 wavenumber bins per decade to obtain the spectra. Because of the large number of transects, formal error bars are very small.

For comparison, we use altimetric measurements of the SSH anomaly as distributed by AVISO [multimission along-track delayed-time product—the altimeter product was produced by Segment Sol multimissions d'ALTimétrie, d'Orbitographie et de localisation precise (SSALTO)/Data Unification and Altimeter Combination System (DUACS) and distributed by AVISO with support from the Centre National d'Études Spatiales (CNES); http://www.aviso.oceanobs.com/duacs/]. The transverse surface velocity is calculated from the along-track SSH gradient assuming geostrophic balance. The power spectra of the transverse velocity presented below are averages over all track segments of the arcs 50 and 126 that lie in a $7° \times 8°$ box centered at 35°N, 68.5°W (years 1993–2002). These track segments nearly parallel the Oleander ship tracks (Fig. 2).

b. Analysis

We analyze kinetic energy spectra at two depths: one in the mixed layer and one in the thermocline. Kinetic energy levels in the mixed layer are slightly higher than in the thermocline (Fig. 5). At scales between 200 and 20 km, both the longitudinal and transverse spectra (solid red and blue in Fig. 5) fall off steeply, with a slope close to -3, both in the mixed layer and the thermocline. The transverse spectra are about three times larger than the longitudinal ones, which is consistent with a two-dimensional isotropic flow, because, for $\mathcal{K}_k^L \sim k^{-3}$, relation (2) yields $\mathcal{K}_k^T = 3\mathcal{K}_k^L$. These characteristics—the slope and the relation between longitudinal and transverse spectra—are consistent with the theoretical predictions for homogeneous, isotropic interior-QG turbulence reviewed in section 2. The slight decay of energy levels with depth is consistent with deep vertical modes. Tulloch et al. (2011) found that the scale of the most unstable baroclinic mode in this region is considerably larger than the deformation scale of about 150 km, consistent with the -3 slope extending to scales as large as 200 km.

At scales larger than 100 km, the transverse kinetic energy spectrum in the mixed layer matches the one

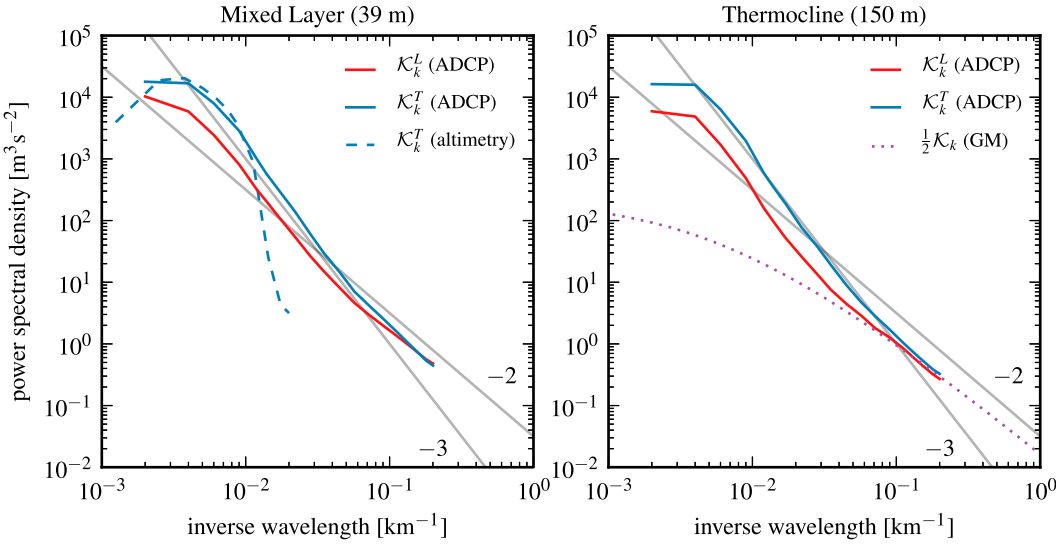

FIG. 5. Gulf Stream region wavenumber spectra of longitudinal and transverse kinetic energies $\mathcal{K}_k^L$ and $\mathcal{K}_k^T$ in the (left) mixed layer (39-m depth) and (right) thermocline (150-m depth) from in situ observations (ADCP). The wavenumber spectrum of surface transverse kinetic energy $\mathcal{K}_k^T$ from altimetry (left) and the GM model spectrum for kinetic energy $\mathcal{K}_k$ in the thermocline (right) are also shown. In both panels, lines with slopes −2 and −3 are given for reference (gray solid lines). Confidence intervals are too small to be visible.

derived from altimetry (dashed blue in Fig. 5). Below 100 km, the altimetric spectrum rolls off much more steeply than the in situ spectrum, but this range of scales is only marginally resolved by altimeters and strongly affected by the smoothing filter applied to remove noise. The match of the in situ and the altimetric spectra is consistent with the flow being predominantly geostrophic and further supports the interpretation in terms of geostrophic turbulence.

In the thermocline, at scales below 20 km, the longitudinal and transverse spectra flatten out, converge, and approach the GM spectrum for a stratification $N = 6 \times 10^{-3}\,\mathrm{s}^{-1}$ taken from the Argo climatology by Roemmich and Gilson (2009) in this region (dotted purple in Fig. 5). This convergence and the fact that $\mathcal{K}_k^L = \mathcal{K}_k^T$ is consistent with internal-wave dynamics and inconsistent with two-dimensional isotropic flow, suggesting that internal waves dominate the kinetic energy at scales below 20 km. The exact match with the GM spectrum may be fortuitous, however, because the interpolation onto a regular grid slightly reduces the spectra at these high wavenumbers, so that they ought to drop below the GM spectrum if only internal-waves were present. A small balanced component may explain the slightly increased spectral amplitudes. Another possible cause of the flattening of the spectra is instrumental noise, but it would be surprising if the instrumental noise just happened to match the amplitude of the internal-wave field. We conclude that the convergence of the longitudinal and transverse spectra and the transition to a flatter slope are a robust result, indicating a change in dynamics. In the mixed layer, the longitudinal and transverse spectra also flatten out and converge, with energy levels slightly higher than in the thermocline. An enhancement of internal-wave energy in the mixed layer is consistent with the vertical structure of low-mode internal waves: thermocline modes project up and can induce increased kinetic energies in the mixed layer, despite the weak stratification (e.g., D'Asaro 1978). It is, however, also possible that some of the excess energy is due to Ekman flows and frontal circulations.

The interpretation of the kinetic energy spectra yields a fairly straightforward picture of submesoscale dynamics in the Gulf Stream region. An interior QG–turbulence regime exists at large scales and an internal-wave regime at small scales, with the transition occurring at about 20 km. We find no evidence of a surface QG–turbulence regime in the upper ocean, which has previously been suggested from analysis of altimetry data from this region (e.g., Le Traon et al. 2008). Enhanced submesoscale energy in the mixed layer, however, may occur in the presence of a deep winter mixed layer, as discussed in section 2e.

6. Subtropical North Pacific

a. Spice dataset

We revisit the Spice dataset presented in Ferrari and Rudnick (2000) to get a better understanding of

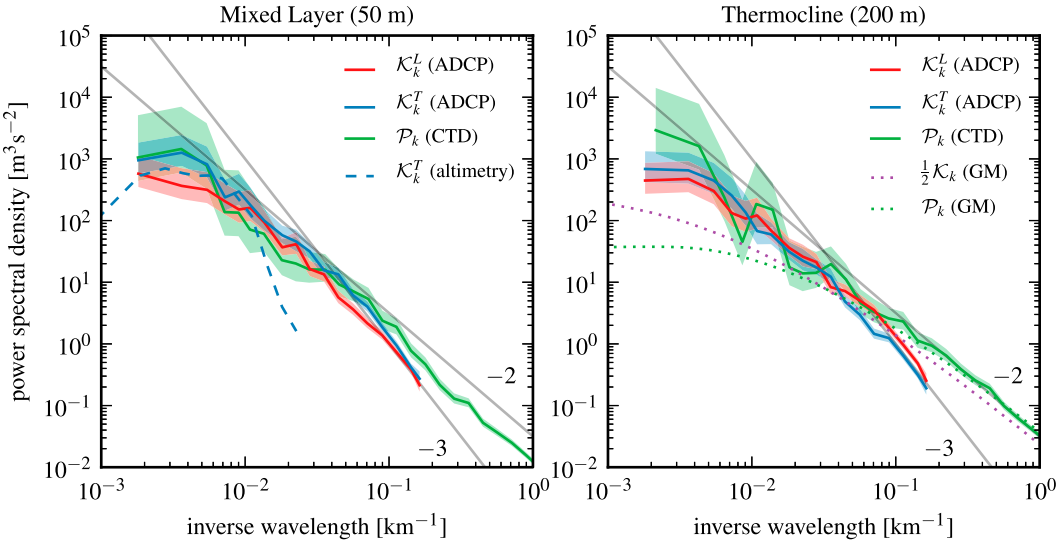

FIG. 6. Subtropical North Pacific wavenumber spectra of longitudinal and transverse kinetic energies $\mathcal{K}_k^L$ and $\mathcal{K}_k^T$ in the mixed layer (50-m depth) and the thermocline (200-m depth) from in situ observations (ADCP, CTD). The wavenumber spectrum of surface transverse kinetic energy $\mathcal{K}_k^T$ from altimetry (left) and the GM model spectra for kinetic and potential energy $\mathcal{K}_k$ and $\mathcal{P}_k$ in the thermocline (right) are also shown. In both panels, lines with slopes −2 and −3 are given for reference (gray solid lines). The shadings show 95% confidence intervals.

submesoscale dynamics in view of recent theoretical developments. The data were collected with a research vessel in successive occupations of the meridian at 140°W between 25° and 35°N (Fig. 2) in the subtropical North Pacific during January and February 1997. We use temperature and salinity from four SeaSoar tows along this transect: a sawtooth profile between 5 and 320 dbar with a period of 12 min, two horizontal tows along the 50 and 200 dbar isobars, and a tow along the 25.5 kg m^{-3} isopycnal. Velocity measurements in the upper 300 m are available from a shipboard ADCP. The velocity measurements and the sawtooth temperature and salinity profiles are averaged into bins of 8-m depth and about 3-km horizontal extent. For the horizontal and isopycnal tows, temperature and salinity are averaged into 10-m bins. See Ferrari and Rudnick (2000) for more detailed information on the data and the rationale behind the scales chosen for the horizontal and vertical averaging. Again, the fast-tow approximation is made. With a ship speed of 4 m s^{-1}, this is slightly less justified than in the Oleander dataset, but geostrophic eddies and the internal-wave continuum remain well resolved. The 7 h it takes to cover 100 km, however, are close to the dominant tidal period—large-scale tidal flows are likely aliased.

The latitude–depth section of density available from the sawtooth profile reveals that the mixed layer has a depth ranging from 100 to 150 m. The 50-dbar horizontal tow is thus within the mixed layer, whereas the 200-dbar horizontal tow is well within the thermocline. The isopycnal tow straddles around the 200-dbar tow at a depth of about 150–250 m—that is, below the mixed layer.

We again compare to AVISO along-track altimetry data. Here, we use all track segments that were collected in February (years 1993–2002) and lie in a 10° × 10° box centered at 30°N, 140°W, the midpoint of the ship track (arcs 19, 95, 106, 171, 182; Fig. 2).

b. *Analysis*

The observations in the subtropical North Pacific do not lend themselves to as simple a dynamical interpretation as those in the Gulf Stream region. We analyze kinetic and potential energy spectra in the mixed layer and the thermocline. The kinetic energy spectra are computed from the ADCP data as before; the potential energy spectra are computed from the horizontal CTD tows, using averaged mixed layer and thermocline values of the stratification N calculated from the sawtooth profile ($N = 2.3 \times 10^{-3}$ s^{-1} in the mixed layer and $N = 8.7 \times 10^{-3}$ s^{-1} in the thermocline).

The kinetic energy levels are similar in mixed layer and thermocline (Fig. 6). At scales larger than 20 km, both the longitudinal and transverse components of kinetic energy (solid red and blue in Fig. 6) are much flatter than in the Gulf Stream region—the slopes are

close to -2.[9] The longitudinal and transverse spectra are similar throughout the observed scales, in both the mixed layer and the thermocline. With a slope of -2, relation (2) predicts $\mathcal{K}_k^T = 2\mathcal{K}_k^L$ for two-dimensional isotropic turbulence, which is not consistent with the observed spectra, but cannot be conclusively rejected because of the rather large error bars. If we interpret this as a violation of (2), one explanation is that the flow is anisotropic. However, an additional transect orthogonal to the ones presented here shows again that transverse and longitudinal kinetic energy spectra are similar—the flow appears to be isotropic. The implication is that the near failure of (2) must stem from a flow that is at least partially horizontally divergent. At scales below 20 km, the kinetic energy spectra are steeper than -2 and fall below the GM spectra (dotted purple in Fig. 6). This is due to the interpolation onto a regular grid: an artificial internal-wave field sampled in the same way as the observations shows the same drop at high wavenumbers.

At scales larger than 20 km, the potential energy spectra (solid green in Fig. 6) have similar magnitudes in the mixed layer and thermocline. At both depths, they also have similar magnitudes as the kinetic energy spectra and exhibit a slope close to -2. Energy equipartition $\mathcal{P}_k = \mathcal{K}_k^L + \mathcal{K}_k^T$ is only marginally satisfied within error bars; $\mathcal{K}_k^L + \mathcal{K}_k^T$ is consistently larger than $\mathcal{P}_k$. At scales below 20 km, the thermocline spectrum of potential energy follows the GM spectrum (dotted green in Fig. 6), while the mixed-layer one is significantly reduced, consistent with the interpretation that the spectrum represents internal waves: free thermocline internal-wave modes of buoyancy are evanescent in the mixed layer and must satisfy a zero boundary condition at the surface (rigid lid), so they must decay in the mixed layer. This is in contrast to the free modes of horizontal velocities that, as mentioned earlier, can be enhanced in the mixed layer, because their surface-boundary condition is zero shear.

At scales larger than 100 km, the in situ spectrum of transverse kinetic energy has the same magnitude as the altimetric spectrum (dashed blue in Fig. 6), with slightly more energy in the in situ spectrum. This may be interpreted as evidence that a significant fraction of the flow is in geostrophic balance, but there is also a significant ageostrophic component. This interpretation, however, ignores the possibility that the altimetric spectrum may be contaminated by ageostrophic flow that projects onto SSH.

The analysis so far does not quite support the inference that motions at scales larger than 20 km are geostrophically balanced. The large error bars, however, preclude definite conclusions. It would still be plausible to interpret the -2 slopes of the kinetic and potential energy spectra as signatures of surface-QG turbulence, as suggested by Klein et al. (2008). The -2 slopes, however, apply only to an ocean with constant stratification; surface QG–turbulence theory predicts different slopes in nonconstant stratification (LaCasce 2012). In the appendix, we show that surface QG–turbulence theory predicts flat kinetic energy spectra in the submesoscale range for an ocean with a weakly stratified mixed layer and a vertically decaying stratification in the thermocline. In addition, the theory predicts that surface-QG modes with scales smaller than 100 km should have decayed at 200-m depth in the thermocline. The observations instead show that the kinetic energy spectrum has a slope of -2 across the whole submesoscale range and that the kinetic and potential energy levels are similar in mixed layer and thermocline. The energy must be in deep modes, not in surface-trapped surface-QG modes. The deep modes, however, are not the result of interior-QG turbulence, because the spectra are flatter than -3.

One possible explanation for the failure of geostrophic-turbulence theories, as alluded to earlier, is that the flow may have a significant ageostrophic component at scales larger than 20 km. Because the energy levels exceed the GM spectra at these large scales, five candidates remain: frontal circulations, Ekman flows, mixed layer turbulence, near-inertial oscillations, and internal tides. Ferrari and Rudnick (2000) showed that density fronts are weak in the region. We further find that the in situ vertical shear is much greater than the geostrophic shear in both the mixed layer and the thermocline, which contradicts the interpretation in terms of frontal circulations, because in frontal flows, most of the shear is in the along-front component and thus in geostrophic balance. Ekman flows and mixed layer turbulence are also unlikely to dominate over these scales because these flows decay rapidly below the mixed layer, while the energy levels in the thermocline are observed to be close to those in the mixed layer at these scales. Near-inertial oscillations have a large ratio of kinetic-to-potential energy, while the potential energy is observed to be of the same order as the kinetic energy at all scales. There is instead support for a strong internal-tide field in the region. Richman et al.

[9] More precisely, both -2 and $-5/3$ slopes are consistent with the observations to within error bars. A slope of -2 gives a better fit over a wider range of scales, but we do not attempt to distinguish between these two slopes because this distinction has little impact on the discussion to follow. In contrast, the spectra are clearly inconsistent with a slope of -3. Note, however, that the error bars presented here are formal ones, representing the random error only. Biases due to, for example, a finite tow speed, unresolved scales, and instrument drift are not accounted for. Statements about spectral slopes in what follows are to be understood with these caveats.

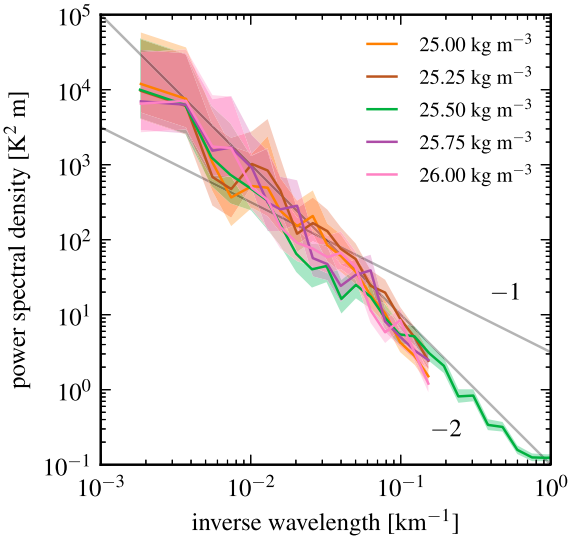

FIG. 7. Subtropical North Pacific temperature spectra along isopycnals interpolated from the sawtooth profile (25.00, 25.25, 25.75, and 26.00 kg m^{-3}) and from the isopycnal tow (25.50 kg m^{-3}). Lines with slopes −1 and −2 are given for reference (gray solid lines). The shadings show 95% confidence intervals.

(2012) ran numerical simulations of the global oceans that resolved both geostrophic eddies and low-mode tides. They found that in regions of low-mesoscale and high-tidal activity, superinertial variability dominates the kinetic energy spectra from scales of a few kilometers to 100 km and larger. Using model output provided by Richman et al., we find that internal tides do indeed dominate the kinetic energy at scales on the order of 100 km in the region under consideration here. Richman et al. (2012) also found that the peaks due to internal tides are considerably broadened, which, together with the superposition with subinertial energy, could explain why no distinct peaks are apparent in the observed spectra.

If internal tides dominate at these large scales, the finite sampling speed is problematic and temporal variations of tidal motions alias into the wavenumber spectra. This prevents a straightforward comparison of model results and observations. More work is required to understand how internal tides project onto spatial scales.

To assess whether geostrophic turbulence is simply masked by unbalanced flow in the energy spectra, we now turn to an analysis of temperature spectra along isopycnals. Temperature fluctuations along isopycnals are fully compensated by salinity and thus behave like a passive tracer (e.g., Ferrari and Rudnick 2000; Smith and Ferrari 2009). These spectra allow inferences about the balanced part of the flow because stirring by internal waves, including internal tides, is essentially filtered out along isopycnals: only the along-isopycnal part of internal-wave motion displaces the weak horizontal temperature gradient.

We calculate temperature spectra along different isopycnals from the CTD tow along the 25.50 kg m^{-3} isopycnal and by interpolating temperature from the sawtooth profile onto isopycnals. The tracer spectra along the different isopycnals, which have a depth range of about 130–250 m, all have very similar variance levels and have slopes close to −2, so there is no change with depth (Fig. 7). Recent observations with gliders in a nearby region confirm this finding: the slopes of passive-tracer spectra remain close to −2 down to 800-m depth (Cole and Rudnick 2012). The slopes are again inconsistent with the vertical decay of surface-QG modes. One would expect that passive-tracer spectra transition, as one moves deeper into the thermocline, from the surface-QG surface spectrum to a flatter Batchelor spectrum at small scales, either because of interior-QG turbulence or nonlocal stirring by large-scale modes (cf., Scott 2006). Given the spectra estimated in the appendix, this transition should be well resolved by the observations, but is not observed. Flows associated with frontal dynamics, as described by semigeostrophy, have a less rapid vertical decay than surface-QG flows and generate −2 spectral slopes (Hoskins and Bretherton 1972; Badin 2012). This may help explain the vertical structure of the tracer spectra, but further study is needed to clarify what spectra frontal dynamics produce at different depths.

Another possible explanation for the failure of geostrophic-turbulence theories is that the assumption of a submesoscale inertial range is violated. Tulloch et al. (2011) suggested that baroclinic instability can inject energy and enstrophy throughout the submesoscale range. They performed a linear stability analysis in the subtropical North Pacific and found that there are submesoscale instabilities, in contrast to strong baroclinic current regions, where instabilities are confined to the mesoscale. The reason for the different instability regimes are the different PV gradient structures. There is a deep reversal of PV gradients in strong baroclinic currents, which induces a Phillips-type instability (Phillips 1954). In quiescent gyres, on the other hand, the instability is more Charney-like, with a surface-buoyancy gradient interacting with an interior-PV gradient, which allows for the growth of small-scale Charney modes (Charney 1947; Tulloch and Smith 2009; Roullet et al. 2012). Capet et al. (2008a) performed high-resolution primitive equation simulations that exhibit submesoscale instabilities. The kinetic and potential energy spectra in these simulations transition from k_h^{-2} near the surface to k_h^{-3} at depth, while the spectrum of temperature remains k_h^{-2}. This indicates that subinertial flows with submesoscale instabilities are capable of producing tracer spectra similar to the ones observed, but again, the mechanisms require further study.

A further possibility is that vertical shear enhances vertical diffusion, which can then act on relatively large

horizontal scales (Haynes and Vanneste 2004; Smith and Ferrari 2009). Further investigation is required to determine whether this mechanism can steepen the spectra from k_h^{-1} to k_h^{-2}.

7. Conclusions

The observations indicate that, in the Gulf Stream region, interior-QG turbulence dominates at scales larger than 20 km, where a transition to internal waves occurs in both the mixed layer and the upper thermocline. In the eastern subtropical North Pacific, geostrophic-turbulence theories fail. There is some indication of a significant unbalanced contribution to the kinetic energy up to scales of 100 km, most likely due to internal tides.

The results in the Gulf Stream region suggest that in a strong baroclinic current, where there are strong interior-PV gradients, a Phillips-type instability creates deep mesoscale modes whose variability is then transferred into the submesoscale through an interior QG–enstrophy cascade. The associated flows dominate the kinetic energy down to scales of tens of kilometers, where internal waves become important. This picture, however, may change substantially in the presence of a deep winter mixed layer. Energetic submesoscale flows can develop and dominate over the interior modes in the mixed layer (e.g., Fox-Kemper et al. 2008; Capet et al. 2008b; Shcherbina et al. 2013).

In quiescent-gyre regions, like the eastern subtropical North Pacific, on the other hand, interior-PV gradients are much weaker. There is still a surface-buoyancy gradient, so one might expect surface-QG dynamics to play a prominent role. But there is no evidence for surface-QG turbulence in the observations: both kinetic energy and tracer spectra are inconsistent with its predictions. Instead, unbalanced flows appear to make a leading-order contribution to the energy throughout the submesoscale range. Passive-tracer spectra along isopycnals, which filter out the effect of internal waves, show a -2 slope independent of depth. These tracer spectra indicate that also the balanced part of the flow does not follow predictions of geostrophic-turbulence theories: neither interior- nor surface-QG turbulence can explain this behavior. Small-scale Charney-type instabilities may be important in setting these spectra, but how -2 slopes emerge remains obscure. Another possibility is coupling between surface-buoyancy anomalies and interior-PV anomalies, an aspect of the dynamics considered in neither surface- nor interior-QG turbulence theory. This also warrants further investigation. A third possibility is that the tracer spectra are modified by shear-enhanced diffusion.

We found that previous claims that kinetic energy spectra with a $-5/3$ slope are telltale signatures of surface-QG dynamics failed to take into account the role of the mixed layer. The presence of a weakly stratified layer in the upper ocean acts to flatten the surface-QG kinetic energy spectra in the submesoscale range between the first baroclinic deformation scale on the order of 100 km and the mixed layer deformation scale on the order of 10 km. Surface QG theory also ignores the strong PV gradient at the mixed layer base, which may introduce Eady-like dynamics in the mixed layer. Our analysis suggests that -2 spectral slopes in kinetic energy spectra can also be associated with a variety of unbalanced processes like internal tides. Clearly, the question of what sets the spectra of kinetic and potential energies at the ocean surface has not yet been fully answered.

That ageostrophic flows may be important near the surface in regions of weak-mesoscale eddy activity has implications for attempts to retrieve the surface flow with altimeters, especially for the upcoming Surface Water and Ocean Topography (SWOT) mission that is expected to resolve SSH fluctuations down to scales of 10 km (e.g., Fu and Ferrari 2008). Two problems come to the fore: (i) if the ageostrophic flow can project significantly onto SSH, it will contaminate the geostrophic surface–velocity estimates and (ii) if the ageostrophic flow has no significant SSH expression, it will need to be inferred through other instruments, because it apparently contributes significantly to the surface velocities.

Acknowledgments. We are thankful for fruitful discussions with Malte Jansen, Joseph H. LaCasce, Ross Tulloch, and Carl Wunsch. We thank Brian K. Arbic, Jay F. Shriver, and James G. Richman for providing us with HYCOM model output. This work was supported by NSF through OCE 1024198 and by ONR through N000140910458.

APPENDIX

Surface QG–Turbulence Predictions of Wavenumber Spectra and Their Vertical Dependence for Non-Constant Stratification

In theories of surface-QG turbulence (Blumen 1978; Lapeyre and Klein 2006), stratification is usually assumed to be constant. Below the injection scale, which is thought to be the mesoscale with its baroclinic instability, there is an enstrophy cascade, in which the surface–potential energy spectrum scales like $\mathcal{P}_{k_h}(0) \sim k_h^{-5/3}$. With constant stratification, the surface–kinetic energy spectrum then also scales like $\mathcal{K}_{k_h}(0) \sim k_h^{-5/3}$ throughout the enstrophy cascade

range. The ocean, however, has highly nonconstant stratification, with an approximately exponential stratification in the thermocline and a weakly stratified mixed layer on top. LaCasce (2012) pointed out that in an ocean with exponential stratification and finite depth, the $k_h^{-5/3}$ surface–potential energy spectrum translates into a surface–kinetic energy spectrum that changes slope. Here, we consider a similar case with parameters appropriate for comparison with our observations in the subtropical North Pacific. Furthermore, we consider how the presence of a mixed layer changes the spectra. Because our observations span a range of depths below the surface, we also compute the vertical dependence of the spectra predicted by surface-QG turbulence. In constant stratification, small-scale modes decay faster in the vertical than large-scale modes, so spectra at depth fall off steeply at small scales (Scott 2006). We extend this result to nonconstant stratification.

To recapitulate the result of Scott, let us start with the case of constant stratification. For simplicity, we consider an infinitely deep ocean, to avoid the introduction of an additional length scale associated with the depth of the ocean. The spectral surface QG–streamfunction $\hat{\psi}$ is then found by inverting the zero interior-PV condition (e.g., Blumen 1978; Lapeyre and Klein 2006)

$$-k_h^2\hat{\psi} + \frac{d}{dz}\left(\frac{f^2}{N^2}\frac{d\hat{\psi}}{dz}\right) = 0, \quad f\frac{d\hat{\psi}}{dz}(0) = \hat{b}(0), \quad \text{and} \quad \hat{\psi}(-\infty) = 0, \tag{A1}$$

which gives, for constant N,

$$\hat{\psi}(z) = \frac{\hat{b}(0)}{Nk_h}e^{Nk_h z/f} \tag{A2}$$

and the kinetic and potential energy spectra are

$$\mathcal{K}_{k_h}(z) = \mathcal{P}_{k_h}(z) = \mathcal{P}_{k_h}(0)e^{2Nk_h z/f}. \tag{A3}$$

These spectra are shown in Fig. 3 (top left), using the stratification $N = 8.7 \times 10^{-3}\,\mathrm{s}^{-1}$ observed at 200-m depth in the subtropical North Pacific. There is an equipartition between kinetic and potential energy at all scales. At a certain depth z, the spectra follow the surface–potential energy spectrum at scales large enough for the modes to penetrate to this depth, that is, at scales larger than the deformation scale associated with z, $k_h \ll -f/Nz$. Around $k_h = -f/Nz$, the spectra fall off sharply because smaller-scale modes do not reach this depth.

For exponential stratification $N = N_0\exp(z/d)$ and again an infinitely deep ocean, the surface-QG streamfunction is (cf. LaCasce 2012)

$$\hat{\psi}(z) = \frac{\hat{b}(0)}{N_0 k_h}\frac{I_1(\mu e^{z/d})}{I_0(\mu)}e^{z/d}, \tag{A4}$$

where the I_α are modified Bessel functions of the first kind and $\mu = N_0 k_h d/f$. The kinetic and potential energy spectra are

$$\mathcal{K}_{k_h}(z) = \mathcal{P}_{k_h}(0)\left[\frac{I_1(\mu e^{z/d})}{I_0(\mu)}e^{z/d}\right]^2 \quad \text{and}$$
$$\mathcal{P}_{k_h}(z) = \mathcal{P}_{k_h}(0)\left[\frac{I_0(\mu e^{z/d})}{I_0(\mu)}e^{z/d}\right]^2. \tag{A5}$$

These are shown in Fig. 3 (top right) with $d = 600\,\mathrm{m}$, which is representative of the subtropical North Pacific thermocline, and N_0 chosen such that the stratification matches the observed thermocline value $N = 8.7 \times 10^{-3}\,\mathrm{s}^{-1}$ at 200-m depth. Let us consider the surface spectra first. For scales that are small compared to the deformation scale associated with the depth scale of stratification d, $k_h \gg f/N_0 d$, the kinetic and potential energy spectra are equal because $I_1(\mu)/I_0(\mu) \approx 1$ for $\mu \gg 1$. In this range, the spectra behave in the same way as with constant stratification.[A1] At scales larger than the deformation scale, $k_h \ll f/N_0 d$, however, the surface–kinetic energy spectrum is

$$\mathcal{K}_{k_h}(0) \approx \frac{N_0^2 k_h^2 d^2}{4f^2}\mathcal{P}_{k_h}(0), \tag{A6}$$

because $I_1(\mu)/I_0(\mu) \approx \mu/2$ for $\mu \ll 1$. The surface–kinetic energy spectrum in this range of scales is therefore much smaller than the potential energy spectrum and has a different slope—the equipartition between kinetic and potential energy is broken. Below the surface, as with constant stratification, the spectra fall off at small scales because modes decay away from the surface.

The presence of a mixed layer also modifies the energy spectra. To demonstrate this, we consider a mixed layer of depth h with constant stratification N_{ML} overlying an infinitely deep ocean, which also has constant but higher stratification N_{TH}. The surface-QG streamfunction for this case is

[A1] This can also be rationalized by WKB arguments. If the modes are shallow enough to not feel the change in stratification, they behave as if the stratification were constant.

$$\hat{\psi}(z) = \begin{cases} \dfrac{\hat{b}(0)}{N_{\mathrm{ML}} k_h} \dfrac{N_{\mathrm{TH}} \sinh \dfrac{N_{\mathrm{ML}} k_h (z+h)}{f} + N_{\mathrm{ML}} \cosh \dfrac{N_{\mathrm{ML}} k_h (z+h)}{f}}{N_{\mathrm{TH}} \cosh \dfrac{N_{\mathrm{ML}} k_h h}{f} + N_{\mathrm{ML}} \sinh \dfrac{N_{\mathrm{ML}} k_h h}{f}} & z > -h \quad \text{and} \\ \dfrac{\hat{b}(0)}{k_h} \dfrac{e^{N_{\mathrm{TH}} k_h (z+h)/f}}{N_{\mathrm{TH}} \cosh \dfrac{N_{\mathrm{ML}} k_h h}{f} + N_{\mathrm{ML}} \sinh \dfrac{N_{\mathrm{ML}} k_h h}{f}} & z < -h, \end{cases} \tag{A7}$$

and the kinetic and potential energy spectra are

$$\mathcal{K}_{k_h}(z) = \begin{cases} \mathcal{P}_{k_h}(0) \left[\dfrac{N_{\mathrm{TH}} \sinh \dfrac{N_{\mathrm{ML}} k_h (z+h)}{f} + N_{\mathrm{ML}} \cosh \dfrac{N_{\mathrm{ML}} k_h (z+h)}{f}}{N_{\mathrm{TH}} \cosh \dfrac{N_{\mathrm{ML}} k_h h}{f} + N_{\mathrm{ML}} \sinh \dfrac{N_{\mathrm{ML}} k_h h}{f}} \right]^2 & z > -h \quad \text{and} \\ \mathcal{P}_{k_h}(0) \left[\dfrac{N_{\mathrm{ML}} e^{N_{\mathrm{TH}} k_h (z+h)/f}}{N_{\mathrm{TH}} \cosh \dfrac{N_{\mathrm{ML}} k_h h}{f} + N_{\mathrm{ML}} \sinh \dfrac{N_{\mathrm{ML}} k_h h}{f}} \right]^2 & z < -h, \quad \text{and} \end{cases} \tag{A8}$$

$$\mathcal{P}_{k_h}(z) = \begin{cases} \mathcal{P}_{k_h}(0) \left[\dfrac{N_{\mathrm{TH}} \cosh \dfrac{N_{\mathrm{ML}} k_h (z+h)}{f} + N_{\mathrm{ML}} \sinh \dfrac{N_{\mathrm{ML}} k_h (z+h)}{f}}{N_{\mathrm{TH}} \cosh \dfrac{N_{\mathrm{ML}} k_h h}{f} + N_{\mathrm{ML}} \sinh \dfrac{N_{\mathrm{ML}} k_h h}{f}} \right]^2 & z > -h \quad \text{and} \\ \mathcal{P}_{k_h}(0) \left[\dfrac{N_{\mathrm{ML}} e^{N_{\mathrm{TH}} k_h (z+h)/f}}{N_{\mathrm{TH}} \cosh \dfrac{N_{\mathrm{ML}} k_h h}{f} + N_{\mathrm{ML}} \sinh \dfrac{N_{\mathrm{ML}} k_h h}{f}} \right]^2 & z < -h. \end{cases} \tag{A9}$$

These are shown in Fig. 3 (bottom left) for $N_{\mathrm{ML}} = 2.3 \times 10^{-3}\,\mathrm{s}^{-1}$ and $N_{\mathrm{TH}} = 8.7 \times 10^{-3}\,\mathrm{s}^{-1}$, the values observed at 50- and 200-m depth, and $h = 100$ m, approximately the observed mixed layer depth. The surface–kinetic energy spectrum again follows the potential energy spectrum at small scales, where modes decay within the mixed layer, but it transitions to a lower level at large scales, where modes are much deeper than the mixed layer and the thermocline stratification dominates the mode structure. This transition occurs around the deformation scale associated with the depth of the mixed layer $N_{\mathrm{ML}}h/f$. In the thermocline, energy levels are drastically reduced because of the jump to higher stratification at the base of the mixed layer.

Let us now combine a mixed layer of depth h and constant stratification N_{ML} with exponential stratification $N = N_0 \exp(z/d)$ below, yielding a somewhat realistic stratification profile. The surface-QG streamfunction for this case is

$$\hat{\psi}(z) = \begin{cases} \dfrac{\hat{b}(0)}{N_{\mathrm{ML}} k_h} \dfrac{N_0 e^{-h/d} \sinh \dfrac{N_{\mathrm{ML}} k_h (z+h)}{f} I_0(\mu e^{-h/d}) + N_{\mathrm{ML}} \cosh \dfrac{N_{\mathrm{ML}} k_h (z+h)}{f} I_1(\mu e^{-h/d})}{N_0 e^{-h/d} \cosh \dfrac{N_{\mathrm{ML}} k_h h}{f} I_0(\mu e^{-h/d}) + N_{\mathrm{ML}} \sinh \dfrac{N_{\mathrm{ML}} k_h h}{f} I_1(\mu e^{-h/d})} & z > -h \quad \text{and} \\ \dfrac{\hat{b}(0)}{k_h} \dfrac{I_1(\mu e^{z/d})}{N_0 e^{-h/d} \cosh \dfrac{N_{\mathrm{ML}} k_h h}{f} I_0(\mu e^{-h/d}) + N_{\mathrm{ML}} \sinh \dfrac{N_{\mathrm{ML}} k_h h}{f} I_1(\mu e^{-h/d})} e^{(z+h)/d} & z < -h, \end{cases} \tag{A10}$$

and the kinetic and potential energy spectra are

$$\mathcal{K}_{k_h}(z) = \begin{cases} \mathcal{P}_{k_h}(0)\left[\dfrac{N_0 e^{-h/d}\sinh\dfrac{N_{\rm ML}k_h(z+h)}{f} I_0(\mu e^{-h/d}) + N_{\rm ML}\cosh\dfrac{N_{\rm ML}k_h(z+h)}{f} I_1(\mu e^{-h/d})}{N_0 e^{-h/d}\cosh\dfrac{N_{\rm ML}k_h h}{f} I_0(\mu e^{-h/d}) + N_{\rm ML}\sinh\dfrac{N_{\rm ML}k_h h}{f} I_1(\mu e^{-h/d})}\right]^2 & z > -h \quad \text{and} \\ \mathcal{P}_{k_h}(0)\left[\dfrac{N_{\rm ML} I_1(\mu e^{z/d})}{N_0 e^{-h/d}\cosh\dfrac{N_{\rm ML}k_h h}{f} I_0(\mu e^{-h/d}) + N_{\rm ML}\sinh\dfrac{N_{\rm ML}k_h h}{f} I_1(\mu e^{-h/d})} e^{(z+h)/d}\right]^2 & z < -h, \quad \text{and} \end{cases} \tag{A11}$$

$$\mathcal{P}_{k_h}(z) = \begin{cases} \mathcal{P}_{k_h}(0)\left[\dfrac{N_0 e^{-h/d}\cosh\dfrac{N_{\rm ML}k_h(z+h)}{f} I_0(\mu e^{-h/d}) + N_{\rm ML}\sinh\dfrac{N_{\rm ML}k_h(z+h)}{f} I_1(\mu e^{-h/d})}{N_0 e^{-h/d}\cosh\dfrac{N_{\rm ML}k_h h}{f} I_0(\mu e^{-h/d}) + N_{\rm ML}\sinh\dfrac{N_{\rm ML}k_h h}{f} I_1(\mu e^{-h/d})}\right]^2 & z > -h \quad \text{and} \\ \mathcal{P}_{k_h}(0)\left[\dfrac{N_{\rm ML} I_0(\mu e^{z/d})}{N_0 e^{-h/d}\cosh\dfrac{N_{\rm ML}k_h h}{f} I_0(\mu e^{-h/d}) + N_{\rm ML}\sinh\dfrac{N_{\rm ML}k_h h}{f} I_1(\mu e^{-h/d})} e^{(z+h)/d}\right]^2 & z < -h. \end{cases} \tag{A12}$$

The spectra shown in Fig. 3 (bottom right), again using parameters appropriate for the subtropical North Pacific, exhibit the combined effect of exponential stratification and a mixed layer: there is a flattening of the kinetic energy spectra at large scales owing to the exponential stratification, potential energy levels in the mixed layer are much higher than in the thermocline, mixed layer kinetic energy spectra transition from the potential energy spectra at small scales to lower energy levels at large scales, and all spectra at depth fall off steeply at small scales.

To make a connection with the observations, we transform the two-dimensional isotropic spectra to one-dimensional spectra using (1) and compute both longitudinal and transverse kinetic energy spectra (Fig. 4). The overall shape of the spectra is similar to the associated two-dimensional isotropic spectra, with slight modifications where the spectra are flat. The longitudinal and transverse kinetic energy spectra still obey (2)—but for nonconstant slopes, they are not separated by a constant factor anymore.

This analysis shows that taking both nonconstant stratification and the vertical decay of modes into account leads to surface QG–turbulence predictions of energy spectra at depths of 50 and 200 m that do not exhibit $k^{-5/3}$ power laws anywhere in the submesoscale range. Even the surface–kinetic energy spectrum does not exhibit this scaling throughout the submesoscale range: it is much flatter at scales larger than 10 km. It should also be noted that throughout the submesoscale range, both kinetic and potential energy levels are predicted to drop significantly going from the mixed layer into the thermocline.

The discussion in this appendix follows a literal interpretation of surface-QG turbulence. The jump in stratification at the base of the mixed layer, however, is associated with a large PV gradient and may act like a surface itself (Smith and Bernard 2013). Such a scenario could be represented with a simplified model consisting of two constant-PV layers—the mixed layer and the thermocline—joined by an interface at the base of the mixed layer. This model will produce different modal structures and energy spectra than that considered above, but it remains to be addressed whether these match the observations.

REFERENCES

Arbic, B. K., J. G. Richman, J. F. Shriver, P. G. Timko, E. J. Metzger, and A. J. Wallcraft, 2012: Global modeling of internal tides within an eddying ocean general circulation model. *Oceanography,* **25,** 20–29, doi:10.5670/oceanog.2012.38.

Badin, G., 2012: Surface semi-geostrophic dynamics in the ocean. *Geophys. Astrophys. Fluid Dyn.,* 1–15, doi:10.1080/03091929.2012.740479.

Batchelor, G. K., 1953: *The Theory of Homogeneous Turbulence.* Cambridge University Press, 197 pp.

Blumen, W., 1978: Uniform potential vorticity flow: Part I. Theory of wave interactions and two-dimensional turbulence. *J. Atmos. Sci.,* **35,** 774–783.

——, 1979: On short-wave baroclinic instability. *J. Atmos. Sci.,* **36,** 1925–1933.

Boccaletti, G., R. Ferrari, and B. Fox-Kemper, 2007: Mixed layer instabilities and restratification. *J. Phys. Oceanogr.,* **37,** 2228–2250.

Boyd, J. P., 1992: The energy spectrum of fronts: Time evolution of shocks in Burgers' equation. *J. Atmos. Sci.,* **49,** 128–139.

Capet, X., P. Klein, B. L. Hua, G. Lapeyre, and J. C. Mcwilliams, 2008a: Surface kinetic energy transfer in surface quasigeostrophic flows. *J. Fluid Mech.,* **604,** 165–174, doi:10.1017/S0022112008001110.

——, J. C. McWilliams, M. J. Molemaker, and A. F. Shchepetkin, 2008b: Mesoscale to submesoscale transition in the California Current System. Part I: Flow structure, eddy flux, and observational tests. *J. Phys. Oceanogr.,* **38,** 29–43.

Charney, J. G., 1947: The dynamics of long waves in a baroclinic westerly current. *J. Meteor.,* **4,** 135–162.

——, 1971: Geostrophic turbulence. *J. Atmos. Sci.,* **28,** 1087–1095.

Cole, S. T., and D. L. Rudnick, 2012: The spatial distribution and annual cycle of upper-ocean thermohaline structure. *J. Geophys. Res.,* **117,** C02027, doi:10.1029/2011JC007033.

D'Asaro, E. A., 1978: Mixed layer velocities induced by internal waves. *J. Geophys. Res.,* **83** (C5), 2437–2438.

Dushaw, B. D., B. D. Cornuelle, P. F. Worcester, B. M. Howe, and D. S. Luther, 1995: Barotropic and baroclinic tides in the central North Pacific Ocean determined from long-range reciprocal acoustic transmissions. *J. Phys. Oceanogr.,* **25,** 631–647.

Emanuel, K. A., 1994: *Atmospheric Convection.* Oxford University Press, 580 pp.

Ferrari, R., and D. L. Rudnick, 2000: Thermohaline variability in the upper ocean. *J. Geophys. Res.,* **105** (C7), 16 857–16 883.

Fox-Kemper, B., R. Ferrari, and R. W. Hallberg, 2008: Parameterization of mixed layer eddies. Part I: Theory and diagnosis. *J. Phys. Oceanogr.,* **38,** 1145–1165.

Frankignoul, C., and P. Müller, 1979: Quasi-geostrophic response of an infinite β-plane ocean to stochastic forcing by the atmosphere. *J. Phys. Oceanogr.,* **9,** 104–127.

Fu, L.-L., and R. Ferrari, 2008: Observing oceanic submesoscale processes from space. *Eos, Trans. Amer. Geophys. Union,* **89,** 489–499, doi:10.1029/2008EO480003.

Garrett, C., 2001: What is the near-inertial band and why is it different from the rest of the internal wave spectrum? *J. Phys. Oceanogr.,* **31,** 962–971.

——, and W. H. Munk, 1972: Space–time scales of internal waves. *Geophys. Fluid Dyn.,* **3,** 225–264, doi:10.1080/03091927208236082.

——, and ——, 1975: Space–time scales of internal waves: A progress report. *J. Geophys. Res.,* **80,** 291–297.

Haine, T., and J. Marshall, 1998: Gravitational, symmetric, and baroclinic instability of the ocean mixed layer. *J. Phys. Oceanogr.,* **28,** 634–658.

Haynes, P. H., and J. Vanneste, 2004: Stratospheric tracer spectra. *J. Atmos. Sci.,* **61,** 161–178.

Hoskins, B. J., and F. P. Bretherton, 1972: Atmospheric frontogenesis models: Mathematical formulation and solution. *J. Atmos. Sci.,* **29,** 11–37.

Kantha, L. H., and C. A. Clayson, 2000: *Small Scales Processses in Geophysical Fluid Flows.* Academic Press, 750 pp.

Katz, E. J., 1973: Profile of an isopycnal surface in the main thermocline of the Sargasso Sea. *J. Phys. Oceanogr.,* **3,** 448–457.

Klein, P., B. L. Hua, G. Lapeyre, X. Capet, S. Le Gentil, and H. Sasaki, 2008: Upper-ocean turbulence from high-resolution 3D simulations. *J. Phys. Oceanogr.,* **38,** 1748–1763.

Klymak, J. M., and J. N. Moum, 2007: Oceanic isopycnal slope spectra. Part I: Internal waves. *J. Phys. Oceanogr.,* **37,** 1215–1231.

LaCasce, J. H., 2012: Surface quasigeostrophic solutions and baroclinic modes with exponential stratification. *J. Phys. Oceanogr.,* **42,** 569–580.

Lapeyre, G., and P. Klein, 2006: Dynamics of the upper oceanic layers in terms of surface quasigeostrophy theory. *J. Phys. Oceanogr.,* **36,** 165–176.

Leith, C. E., 1971: Atmospheric predictability and two-dimensional turbulence. *J. Atmos. Sci.,* **28,** 145–161.

Le Traon, P. Y., P. Klein, B. L. Hua, and G. Dibarboure, 2008: Do altimeter wavenumber spectra agree with the interior or surface quasigeostrophic theory? *J. Phys. Oceanogr.,* **38,** 1137–1142.

Lvov, Y., K. Polzin, and E. Tabak, 2004: Energy spectra of the oceans internal wave field: Theory and observations. *Phys. Rev. Lett.,* **92,** 1–4.

Molemaker, M. J., J. C. McWilliams, and X. Capet, 2010: Balanced and unbalanced routes to dissipation in an equilibrated Eady flow. *J. Fluid Mech.,* **654,** 35–63, doi:10.1017/S0022112009993272.

Munk, W. H., 1981: Internal waves and small-scale processes. *Evolution of Physical Oceanography,* B. A. Warren and C. Wunsch, Eds., The MIT Press, 264–291.

Niiler, P. P., 1969: On the Ekman divergence in an oceanic jet. *J. Geophys. Res.,* **74,** 7048–7052.

Phillips, N. A., 1954: Energy transformations and meridional circulations associated with simple Baroclinic waves in a two-level, quasigeostrophic model. *Tellus,* **6,** 273–286, doi:10.1111/j.2153-3490.1954.tb01123.x.

Pollard, R. T., 1970: On the generation by winds of inertial waves in the ocean. *Deep Sea Res. Oceanogr. Abstr.,* **17,** 795–812, doi:10.1016/0011-7471(70)90042-2.

Ray, R. D., and G. T. Mitchum, 1997: Surface manifestation of internal tides in the deep ocean: Observations from altimetry and island gauges. *Prog. Oceanogr.,* **40** (1–4), 135–162, doi:10.1016/S0079-6611(97)00025-6.

Richman, J. G., B. K. Arbic, J. F. Shriver, E. J. Metzger, and A. J. Wallcraft, 2012: Inferring dynamics from the wavenumber spectra of an eddying global ocean model with embedded tides. *J. Geophys. Res.,* **117,** C12012, doi:10.1029/2012JC008364.

Roemmich, D., and J. Gilson, 2009: The 2004–2008 mean and annual cycle of temperature, salinity, and steric height in the global ocean from the Argo Program. *Prog. Oceanogr.,* **82,** 81–100, doi:10.1016/j.pocean.2009.03.004.

Roullet, G., J. C. McWilliams, X. Capet, and M. J. Molemaker, 2012: Properties of steady geostrophic turbulence with isopycnal outcropping. *J. Phys. Oceanogr.,* **42,** 18–38.

Samelson, R. M., and C. A. Paulson, 1988: Towed thermistor chain observations of fronts in the subtropical North Pacific. *J. Geophys. Res.,* **93** (C3), 2237–2246.

Sasaki, H., and P. Klein, 2012: SSH wavenumber spectra in the North Pacific from a high-resolution realistic simulation. *J. Phys. Oceanogr.,* **42,** 1233–1241.

Schmitz, W. J. J., 1988: Exploration of the eddy field in the mid-latitude North Pacific. *J. Phys. Oceanogr.,* **18,** 459–468.

Scott, R. K., 2006: Local and nonlocal advection of a passive scalar. *Phys. Fluids,* **18,** 116601, doi:10.1063/1.2375020.

Shcherbina, A. Y., E. A. D'Asaro, C. M. Lee, J. M. Klymak, M. J. Molemaker, and J. C. McWilliams, 2013: Statistics of vertical vorticity, divergence, and strain in a developed submesoscale turbulence field. *Geophys. Res. Lett.,* **40,** doi:10.1002/grl.50919, in press.

Smith, K. S., and R. Ferrari, 2009: The production and dissipation of compensated thermohaline variance by mesoscale stirring. *J. Phys. Oceanogr.,* **39,** 2477–2501.

——, and E. Bernard, 2013: Geostrophic turbulence near rapid changes in stratification. *Phys. Fluids,* **25,** 046601, doi:10.1063/1.4799470.

Stammer, D., 1997: Global characteristics of ocean variability estimated from regional TOPEX/Poseidon altimeter measurements. *J. Phys. Oceanogr.,* **27,** 1743–1769.

Tulloch, R., and K. S. Smith, 2009: Quasigeostrophic turbulence with explicit surface dynamics: Application to the atmospheric energy spectrum. *J. Atmos. Sci.,* **66,** 450–467.

——, J. Marshall, C. Hill, and K. S. Smith, 2011: Scales, growth rates, and spectral fluxes of baroclinic instability in the ocean. *J. Phys. Oceanogr.,* **41,** 1057–1076.

Vallis, G. K., 2006: *Atmospheric and Ocean Fluid Dynamics.* Cambridge University Press, 745 pp.

Wang, D.-P., C. N. Flagg, K. Donohue, and H. T. Rossby, 2010: Wavenumber spectrum in the Gulf Stream from shipboard ADCP observations and comparison with altimetry measurements. *J. Phys. Oceanogr.,* **40,** 840–844.

Wunsch, C., and D. Stammer, 1998: Satellite altimetry, the marine geoid, and the oceanic general circulation. *Annu. Rev. Fluid Mech.,* **26,** 219–253, doi:10.1146/annurev.earth.26.1.219.

Xu, Y., and L.-L. Fu, 2011: Global variability of the wavenumber spectrum of oceanic mesoscale turbulence. *J. Phys. Oceanogr.,* **41,** 802–809.

——, and ——, 2012: The effects of altimeter instrument noise on the estimation of the wavenumber spectrum of sea surface height. *J. Phys. Oceanogr.,* **42,** 2229–2233.

Zhao, Z., M. H. Alford, and J. B. Girton, 2012: Mapping low-mode internal tides from multisatellite altimetry. *Oceanography,* **25,** 42–51, doi:10.5670/oceanog.2012.40.